EUROPEAN ORGANIZATION FOR NUCLEAR RESEARCH

CERN-EP/85-101
27 June 1985

HIGH TRANSVERSE ENERGY AND HIGH TRANSVERSE MOMENTUM EVENTS IN $p\bar{p}$ AND pp INTERACTIONS AT THE CERN INTERSECTING STORAGE RINGS

CERN[1]-Michigan State[2]-Oxford[3]-Rockefeller[4] (CMOR) Collaboration

A.L.S. Angelis[3], G. Basini[1,*], H.-J. Besch[1], R.E. Breedon[4], L. Camilleri[1], T.J. Chapin[4], R.L. Cool[4], P.T. Cox[1,4], C. von Gagern[1,4,**], C. Grosso-Pilcher[1,***], D.S. Hanna[1,4,†], B.M. Humphries[2], J.T. Linnemann[4,2], C. Newman-Holmes[1,††], R.B. Nickerson[3,†††], N. Phinney[1,3,#], B.G. Pope[2], S.H. Pordes[1,4,††], K.J. Powell[3], R.W. Rusack[4], C.W. Salgado[2], A.M. Segar[3], S.R. Stampke[2], M.J. Tannenbaum[4,##] and J.M. Yelton[3]

(Submitted to Nucl. Phys.)

---

1) CERN, Geneva, Switzerland
2) Michigan State University, East Lansing, MI, USA
3) Oxford University, Oxford, England
4) Rockefeller University, New York, NY, USA

*) Present address: Laboratori Nazionali dell'INFN, Frascati, Italy
**) Present address: Rohde and Schwarz, Munich, Fed. Rep. Germany
***) Present address: Enrico Fermi Institute, University of Chicago, Chicago, IL, USA
†) Present address: McGill University, Montreal, Quebec, Canada
††) Present address: FNAL, Batavia, IL, USA

ABSTRACT

A comparison between $p\bar{p}$ and pp interactions at $\sqrt{s}$ = 52.7 GeV is presented for a total neutral transverse energy (E_T^0) trigger and for a high transverse momentum (p_T) neutral cluster trigger. The rate of production of events in the range $6 < E_T^0 < 20$ GeV is observed to be 10% higher in $p\bar{p}$ collisions than in pp collisions. A study of the structure of the events shows this excess to be due to more isotropic events being produced in $p\bar{p}$ collisions. The ratio of the production cross-section for single neutral clusters in $p\bar{p}$ and pp interactions in the range $1.25 < p_T < 10$ GeV/c does not significantly differ from unity.

1. INTRODUCTION

The highest $\sqrt{s}$ comparisons between $p\bar{p}$ and pp interactions in the central region have been obtained at the CERN Intersecting Storage Rings (ISR) [1,2]. The ISR had the advantage that because it consisted of two separate rings and magnet systems either two proton beams or a proton and an antiproton beam could be stored in it. The same detectors could then be used to compare $p\bar{p}$ interactions with pp interactions, thus minimizing systematic effects. The data presented here were taken at the CERN ISR in December 1982 and December 1983 at $\sqrt{s}$ = 52.7 GeV with a total neutral energy trigger and with a high transverse momentum neutral cluster trigger.

2. APPARATUS

The apparatus, shown in Fig. 1, consisted of a superconducting solenoid providing a 1.4 T magnetic field surrounding a set of concentric cylindrical drift chambers, DCM1-5. The electromagnetic calorimeter was divided into six azimuthal sextants. Four of the sextants contained a module of lead/scintillator shower counters inside the solenoid. The remaining two sextants each contained one lead-glass module located outside the magnet.

Each shower counter module was 1.5 m long, and subtended 50° in azimuth and $\pm$1.1 units of rapidity y, centred on y = 0, and was segmented azimuthally into eight counters. Each counter was 14 radiation lengths (RL) thick, and consisted of 16 layers of scintillator interleaved with layers of lead. The 4 layers nearest the beam interaction region ('front') and the remaining 12 layers ('back') were independently viewed by phototubes at each end of the counter. The energy of a particle incident on a given shower counter was obtained from the pulse heights recorded in the four phototubes viewing the counter. An estimate of the point of incidence of the particle along the counter was obtained from the differences in amplitude and/or time of arrival of the pulses from the two phototubes viewing the same layers. Each lead-glass module consisted of a front array of 34 blocks, each 4 RL thick, and a back array of 168 blocks, each 17 RL thick, all of type SF5 lead glass. Each lead-glass array

covered ± 0.6 units of rapidity, also centred on $y = 0$. Their azimuthal acceptances were 57° for the back arrays and 45° for the front arrays.

Both the shower counters and lead glass were initially calibrated in an electron beam at the CERN Proton Synchrotron. Subsequently, the calibration of the shower counters and front lead glass was monitored using a system of light flashers (krytrons) connected by fibre optics to the counters and a set of reference counters. The stability of the krytron light output was monitored by comparison in a reference counter with the light output from a NaI crystal on which was mounted a ^{137}Cs source. The calibration of the back glass [3] was monitored with NaI crystals doped with ^{241}Am. All the electromagnetic counters were also monitored using minimum ionizing particles, mainly cosmic-ray initiated muons. The r.m.s energy resolution of the lead glass was $(4.3/\sqrt{E} + 2)\%$, and that of the shower counters was $(16/\sqrt{E})\%$, with E in GeV.

Charged particles were measured over the full azimuth, in the rapidity range ± 1.2 centred on $y = 0$, using the drift chambers. The spatial resolution was about 350 μm, yielding a momentum resolution of $\Delta p_T/p_T = 0.07 p_T$ with p_T in GeV/c. Further details on the solenoid and the drift chambers are available elsewhere [4].

In the forward direction, telescopes of two scintillation counters were located one below and one above the beam pipe on each of the outgoing beams. Each of the telescopes was located 1.4 m from the interaction region and was sensitive to particles emitted with polar angles between 31 and 95 mrad in the laboratory. Any coincidence of two telescopes, one in each arm, defined an event with the forward requirement fulfilled. In our previous publication [1] the forward requirement was used to reduce the background at the trigger level. Since the beam conditions were better in 1982 and 1983, there was no need for this requirement at the trigger level, but the counter information was recorded. These counters were also used to monitor the luminosity.

Finally, there were two hodoscopes of scintillation counters, a barrel hodoscope (A) consisting of 32 azimuthal counters located between the innermost and neighbouring drift chambers, and a hodoscope (B) of 24 azimuthal counters located outside the solenoid, 12 in front of each lead-glass module. Each of these scintillation counters was equipped with a phototube at each end.

3. TOTAL NEUTRAL TRANSVERSE ENERGY

3.1 Event selection

The total neutral energy trigger required the sum of all energies deposited in the shower counters and lead-glass counters to be greater than some threshold. In the off-line analysis this energy threshold was applied again to the total neutral transverse energy E_T^0, after correcting the observed pulse heights using more detailed calibration information.

Table 1 gives the integrated luminosities and the lowest trigger thresholds for the different data sets used.

The comparison of $p\bar{p}$ and pp interactions is sensitive to the efficiency of all cuts applied. Therefore care was taken that the cuts affected all data sets in the same way.

In order to minimize background arising from beam-gas interactions the following cuts were applied to the data. More than three A counters were required to have an energy deposition greater than or equal to that for a minimum ionizing particle. Each event was required to contain at least three charged tracks, with two or more of these tracks intersecting at a point, the vertex, which itself was required to be well within the interaction region. The sum of the longitudinal momenta of all charged tracks had to be within $\pm$12.5 GeV/c with respect to the mean value, which varied by about 1 GeV/c for each set of data.

A small number of events were due to cosmic rays, stray beam protons, particles hitting the NaI crystal of a lead-glass block, or were caused by

electronic problems in one of the analog-to-digital converters (ADCs). They were removed by comparing the energy deposition in the lead-glass arrays within the usual ADC gate and within a much wider gate, by making consistency checks on the pulse heights of the left and right tubes of any shower counter, and by checking the amount of the clustered energy compared with the total unclustered energy.

At high instantaneous luminosities in pp interactions [5] the E_T^0 data were contaminated by triggers originating from an overlap of more than one interaction, each with energy below threshold, occurring during the recording time of the apparatus. Since the instantaneous luminosities for the $p\bar{p}$ interactions and for the corresponding pp comparison runs were considerably lower than the usual ISR instantaneous luminosity, this effect was negligible and no correction was applied.

3.2 Neutral transverse energy spectrum

The total neutral transverse energy E_T^0 of an event was obtained by summing the transverse energy contained in every lead-glass block and shower counter in the centre-of-mass system (c.m.s.), calculated by assuming it was caused by a photon originating at the vertex. A correction for energy loss in the coil was applied to the energies in the lead-glass blocks. The residual background in the data was estimated by varying the vertex cuts and was found to be of the order of 2%. The overall systematic error in the ratios is estimated to be of the order of 4%, arising from uncertainties in the luminosity measurement, residual background, and uneven cut efficiencies and is not included in the statistical errors shown.

The E_T^0 spectra were obtained by dividing the number of events in a given E_T^0 interval by the appropriate integrated luminosity. No corrections were made for resolution, double hits in the same shower counter, or energy deposited by charged tracks in the electromagnetic calorimeter. The data from 1982 and 1983

agree within the statistical errors and have therefore been combined. The E_T^0 spectra for $p\bar{p}$ and pp interactions are shown in Fig. 2. It can be seen that, although the measurements span more than five orders of magnitude, differences between the $p\bar{p}$ and pp spectra are always small. The spectra follow a form $\sim \exp(-1.01E_T^0)$.

In order to obtain the ratio of these two spectra, the $p\bar{p}$ to pp ratios for 1982 and 1983 data were calculated separately and combined afterwards. This minimizes systematic effects since the pp comparison runs for each year were taken close in time to the corresponding $p\bar{p}$ data runs. Any shifts in absolute energy calibration which could be present over a long period of time were eliminated by this method. The ratio of the $p\bar{p}$ and pp E_T^0 spectra is shown in Fig. 3 as a function of E_T^0. A linear fit to the data points, also shown in the figure, results in a value of 1.05 at 6 GeV and 1.18 at 20 GeV with a χ^2/DOF of 0.62. Fitting to a constant $p\bar{p}$/pp ratio yields a value of 1.08 with an equally acceptable χ^2/DOF of 0.92. A fit to a constant ratio of one results in a χ^2/DOF of 3.95.

3.3 Correlation between $p\bar{p}$/pp excess and event structure

Following the method of two-jet analysis described in Ref. [5], each event can be divided into two 'jets'. An event was arbitrarily split into two spatial hemispheres and the sum of momenta of the particles in each was made. The larger of the two sums was used to define another division into two hemispheres, and this procedure repeated until the change in the larger momentum sum was negligible. This sum defined one jet, and the second jet was then defined by the sum of momenta in the opposite hemisphere. Note that these axes were not forced to be 180° apart, and the split into 'jets' was made even for non jet-like events. The relative importance of jet-like and isotropic events in the large transverse energy triggers can be studied through the sphericity variable, S. In this detector it is defined as $S = S_1 + S_2$, where $S_n = 3\Sigma j_{Ti}^2 / 2\Sigma p_i^2$ and n = 1, 2 labelled the two jet axes in the event, p_i was the magnitude of the momentum of

particle i, j_{Ti} its transverse component relative to its jet axis, and the sums were over all particles, charged and neutral, associated with axis n.

Jet-like events have small sphericity and isotropic events have larger sphericity. Our previous analysis [5] of very high luminosity pp data showed a mean sphericity $\langle S \rangle$ that decreased with increasing E_T^0, demonstrating the increasing importance of the two-jet component. Indeed at $E_T^0 \sim 25$ GeV the data consisted almost entirely of jets. Because of the much lower luminosity prevailing during the $p\bar{p}$ running the present data barely reach $E_T^0 \sim 20$ GeV, and are therefore never dominated by jet-like events. Nonetheless here too $\langle S \rangle$ can be seen to decrease with increasing E_T^0 in both the $p\bar{p}$ and pp data (Fig. 4), clearly demonstrating the emergence of the two-jet component in both sets of data.

In order to determine whether the larger event rate observed in $p\bar{p}$ was due to events of particular topology, the events were divided into two sets depending on whether their sphericity was below 0.2 (jet-like) or above 0.2 (isotropic). The ratio of $p\bar{p}$ to pp E_T^0 spectra for low-sphericity events is shown in Fig. 5a. The statistical errors are large since few events are jet-like in this E_T^0 range. A fit to a constant ratio yields a value of 0.98 ± 0.04 and a χ^2 of 0.6/DOF. This is perfectly consistent with unity. On the contrary the $p\bar{p}$ to pp ratio for isotropic events, Fig. 5b, is consistently above unity, with a mean of 1.08 ± 0.01.

Another way to study the relative importance of the two-jet component is to measure the fraction of the E_T^0 of an event contained in the most energetic clusters in the event. For this study the energy in the lead-glass arrays and in the shower counters was clustered. The clustering algorithm allowed up to 4 x 4 blocks of the back lead-glass arrays and added the energy of the corresponding front lead-glass blocks. In the shower counters all neighbouring counters were added into a single cluster if there was no significant dip in the lateral energy flow and if the measured positions along the counters matched. On the average about 2.7 GeV of energy remained unclustered, usually because it

was distributed over many counters, each of which contained less energy than the energy required for a cluster core. This minimum energy was 200 MeV for lead-glass blocks and 500 MeV for shower counters. The transverse energy of the clusters was then denoted by $(\varepsilon_T^0)_n$, where the index n labels the sorted clusters so that $(\varepsilon_T^0)_1$ is the one with the highest transverse momentum. The fraction of the total clustered energy contained in the two most-energetic clusters, $[(\varepsilon_T^0)_1 + (\varepsilon_T^0)_2]/E_T^0$, was formed for each event. Clearly two-jet (two-cluster) events will have large values of this ratio. The mean value of this fraction is shown as a function of E_T^0 in Fig. 6 for the $p\bar{p}$ and pp data separately. The value of this mean in the pp data is observed to start rising steadily above $E_T^0 \sim 10$ GeV, indicating that in an increasingly larger fraction of the events the energy is concentrated in just two clusters or jets. The data for $p\bar{p}$ collisions are systematically below those for pp collisions and do not exhibit as marked a rise as the pp data. This again demonstrates the increased relative importance of the isotropic event component in the $p\bar{p}$ sample.

The mean multiplicity of charged particles was observed to be higher in $p\bar{p}$ collisions than in pp collisions [6]. This increase was traced to an additional event component, referred to as the annihilation component, with a mean multiplicity about 30% higher than the mean pp and $p\bar{p}$ multiplicity, and occurring mostly in the central region. An increase in the two-particle-pseudorapidity correlation function in $p\bar{p}$ collisions over the values measured in pp collisions is also found [7] in the central region. These observations are most likely related to the larger probability of producing isotopic events in $p\bar{p}$ collisions reported here. Collectively these effects can be understood in terms of events due to $p\bar{p}$ annihilation. This process is expected to be highly inelastic and hence of high multiplicity, and to produce more particles centrally since leading particles are not present in annihilation.

3.4 Effects of a forward requirement

The ratio between the E_T^0 spectrum including all events and the spectrum obtained by taking only events where the forward requirement was fulfilled, is

shown in Fig. 7. The forward requirement is seen to be satisfied less frequently as E_T^0 increases. This trend is the same in $p\bar{p}$ and pp interactions. This observation is consistent with the assumption that the higher the E_T^0 in the central region the fewer the particles in the forward direction.

The $p\bar{p}$/pp ratio for events with the forward requirement is very similar to the ratio for all events (Fig. 3), as seen in Fig. 8. It is also in agreement with the data collected in 1981 with this apparatus [1] which are also shown in Fig. 8.

3.5 Charge ratios

The charge ratio N_+/N_- for leading particles in an event is expected to reflect the original beam charge. Since in $p\bar{p}$ the net charge of the beams is zero, this ratio should be unity, whereas for pp interactions the ratio is expected to be above one, because of the total beam charge of two. The leading particle of an event was defined as the charged track with the highest p_T, with the restriction 0.3 GeV/c $< p_T <$ 15 GeV/c. Since this experiment triggered on neutral energy, the leading charged particle usually had a much smaller energy than the E_T^0 of the event. Figure 9 shows the charge ratio for the leaders as a function of E_T^0 both for $p\bar{p}$ and pp interactions. The mean value for $p\bar{p}$ interactions is 0.995 ± 0.009, well in agreement with the expected value of unity. For pp interactions the mean value is 1.192 ± 0.021, with no dependence on E_T^0.

The charge asymmetry $(N_+ - N_-)/(N_+ + N_-)$ is plotted as a function of the rapidity of the leader in Fig. 10. For $p\bar{p}$ interactions the leader is predominantly negative in the hemisphere centred on the outgoing antiproton. This is where fragments from antiquarks scattered out of the antiproton are expected to be found. Conversely the leader is more often positive in the hemisphere centred on the outgoing proton. The charge asymmetry is close to zero at small rapidities as there is no precise separation into a proton and an

antiproton hemisphere. In pp interactions the leader is of course more often positive throughout the whole rapidity range and the charge asymmetry is consistent with being constant as a function of rapidity. The charge asymmetry in the proton hemisphere becomes equal for $p\bar{p}$ and pp interactions for $|y| > 0.6$. Therefore this seems to be the rapidity beyond which one can associate unambiguously a scattered leading particle with a given incident beam. A study of the charge asymmetry as a function of E_T^0 showed it to be essentially independent of E_T^0.

4. NEUTRAL CLUSTER TRIGGER

4.1 Event selection

The high transverse momentum single-particle trigger required an energy above a given threshold being deposited in a restricted cluster of counters. In the sextants equipped with lead-glass blocks a restricted cluster was defined as a cluster of at most 3 x 3 back array blocks, adding in the energy of the corresponding front array blocks, whereas in the shower counters it was defined as two neighbouring counters containing energy above threshold.

Tables 2 and 3 give the integrated luminosities and the lowest thresholds for the different data sets used.

In the off-line analysis the transverse momentum p_T was calculated using more detailed calibration information and assuming the mass of a π^0 when transforming to the c.m.s. This p_T was required to be above the hardware threshold. Other cuts, similar to the ones described for the E_T^0 data, were applied. At least two A counters were required to have been hit.

In the shower-counter sextants energy clusters were required to consist of two counters at most and to be well separated from any nearby cluster. This matched the requirement of the trigger and also reduced the probability of accepting events which originate from several particles hitting neighbouring counters. A π^0 of 5 GeV/c p_T has an average lateral spread of one counter and is therefore well contained within two of them. In the lead-glass sextants a correction for energy loss in the coil was applied.

4.2 Transverse momentum spectra ratios

For the clusters obtained according to the selection just described the invariant cross-sections $Ed^3\sigma/dp^3$ were calculated. The analysis was performed in the shower-counter and in the lead-glass sextants separately. The residual background in the data was estimated to be of the order of 6% by varying the vertex cuts applied. The overall systematic error in the ratios is expected to be of the order of 10% arising from uncertainties in the luminosity measurement, residual background, and uneven cut efficiencies, and is not included in the statistical errors shown.

The cross-sections for both counter types were very similar. Figure 11 shows the invariant cross-sections for pp interactions in the shower counters and in the lead glass. Appropriate cuts in the acceptance were made to ensure full efficiency of the counters. Both parts of the apparatus agree in the p_T range up to 8 GeV/c within a factor of two; however, the spectrum in the lead glass appears to be slightly flatter than that in the shower counters. This can be caused by the different definitions for clusters or by energy calibration differences. The spectrum in the shower counters matches very well a previous measurement [8] which was evaluated in the lead-glass sextants. This spectrum is also presented in Fig. 11 as open triangles. It should be stressed that differences in calibration between different parts of the apparatus will cancel out as $p\bar{p}/pp$ ratios are formed for the lead-glass and the shower-counter sextants separately.

It should be noted that the neutral clusters in this analysis, although dominantly due to π^0's also have a contribution from photons, and from η and other neutral mesons.

Figures 12a and b show the $p\bar{p}/pp$ ratio for lead-glass and shower-counter sextants respectively. The ratios $p\bar{p}/pp$ for these spectra were obtained for 1982 and 1983 data separately, and combined afterwards. Both show a similar

p_T dependence of the $\bar{p}p/pp$ ratio. The ratio obtained by combining lead-glass and shower-counter sextants is shown in Fig. 13. It is consistent with unity except in the range 4-6 GeV/c where there are relatively fewer events in $\bar{p}p$ interactions. The result of calculations [9] based on the Diquark (DQ) and Constituent Interchange Model (CIM) approaches are also shown in Fig. 13. They are in clear disagreement with the data. A Quark-Fusion (QF) calculation predicts a much higher ratio [9] than is observed here. However, appropriate mixtures of QF, CIM, and DQ could be made to agree with the data. Calculations based on QCD predict a ratio of the π^0 yield close to unity throughout the p_T range covered by this experiment, in agreement with our observations. The reason is that in this p_T interval the π^0's are predominantly the fragmentation product of gluons [10] and the gluon structure functions of the proton and antiproton are expected to be the same.

5. CONCLUSIONS

We have shown that the $\bar{p}p/pp$ ratio of the E_T^0 spectra has values in excess of unity in the range $6 < E_T^0 < 20$ GeV. Dividing the data into jet-like events and isotropic events we find that this excess is due to the isotropic events. A fit of the $\bar{p}p/pp$ ratio of E_T^0 spectra for isotropic events yields a value of 1.08 ± 0.01, whereas a similar fit for jet-like events gives a value of 0.98 ± 0.04. This effect is probably due to the annihilation mechanism and can be related to the increased multiplicity and correlations observed in $\bar{p}p$ collisions by other experiments. The $\bar{p}p/pp$ ratio of the p_T spectra for single neutral clusters is consistent with unity in the range $1.25 < p_T < 10$ GeV/c in accordance with QCD calculations.

In conclusion, it appears that the only difference between $\bar{p}p$ and pp interactions at high transverse energy or high transverse momentum can be attributed to isotropic events. Events which originate from a hard scatter (jet or single particles at high p_T) do not exhibit different production rates in $\bar{p}p$ and pp interactions.

Acknowledgements

We thank the staff and management of CERN for their assistance in the successful operation of this experiment, in particular those of the PS, ISR, and DD Divisions. We are grateful to R. Gros for the excellent maintenance of our apparatus, and to M.-A. Huber for her dedicated secretarial and data-management work. We also acknowledge the assistance of A.M. Smith of the CERN EF Division.

REFERENCES

[1] A.L.S. Angelis et al., Phys. Lett. 118B (1982) 217.

[2] T. Åkesson et al., Phys. Lett. 121B (1983) 439;

T. Åkesson et al., Phys. Lett. 129B (1983) 269;

T. Åkesson et al., Nucl. Phys. B228 (1983) 409.

[3] J.S. Beale et al., Nucl. Instrum. Methods 117 (1974) 501.

[4] M. Morpurgo, Cryogenics 17 (1977) 89;

L. Camilleri et al., Nucl. Instrum. Methods 156 (1978) 275.

[5] A.L.S. Angelis et al., Nucl Phys. B244 (1984) 1.

[6] Contribution by experiment R210 in 'Proton-Antiproton Collisions in the ISR', ISR Discussion Meetings, Series 2, Number 5 (CERN).

[7] V. Cavasinni et al., Z. Phys. C 21 (1984) 299.

[8] A.L.S. Angelis et al., Phys. Lett. 79B (1978) 505.

[9] M.K. Chase and W.J. Stirling, Nucl. Phys. B133 (1978) 157.

[10] R. Horgan and M. Jacob, Nucl. Phys. B179 (1981) 441.

Table 1

Integrated luminosities for E_T^0 trigger

Year	Beams	Lowest threshold (GeV)	∫L of all thresholds (cm^{-2})
1982	$p\bar{p}$	6	2.27×10^{33}
1982	pp	6	15.27×10^{33}
1983	$p\bar{p}$	11	6.37×10^{33}
1983	pp	11	205.13×10^{33}

Table 2

Integrated luminosities for lead-glass sextants

Year	Beams	Lowest threshold (GeV)	∫L of all thresholds (cm^{-2})
1982	$p\bar{p}$	1.25	2.30×10^{33}
1982	pp	1.25	21.91×10^{33}
1983	$p\bar{p}$	2.5	6.42×10^{33}
1983	pp	1.875	122.92×10^{33}

Table 3

Integrated luminosities for shower-counter sextants

Year	Beams	Lowest threshold (GeV)	∫L of all thresholds (cm^{-2})
1982	$p\bar{p}$	2.75	2.30×10^{33}
1982	pp	2.75	24.76×10^{33}
1983	$p\bar{p}$	4.375	6.42×10^{33}
1983	pp	3.75	131.22×10^{33}

FIGURE CAPTIONS

Fig. 1 : The apparatus viewed along the beam axes.

Fig. 2 : The events/integrated luminosity spectra as a function of E_T^0 for $p\bar{p}$ (full circles) and pp (crosses). The points are slightly displaced horizontally with respect to each other for clarity.

Fig. 3 : Ratio $p\bar{p}/pp$ for the E_T^0 spectra as a function of E_T^0. The line indicates a linear fit to the data. The horizontal line at unity serves to guide the eye.

Fig. 4 : Mean spericity S as a function of E_T^0 for $p\bar{p}$ and pp interactions. The points are slightly displaced horizontally with respect to each other for clarity.

Fig. 5 : Ratio $p\bar{p}/pp$ for the E_T^0 spectra as a function of E_T^0. The horizontal line at unity serves to guide the eye.

a) Events with sphericity $S < 0.2$,

b) Events with sphericity $S \geq 0.2$.

Fig. 6 : Mean fraction of clustered E_T^0 contained in the two most-energetic clusters as a function of E_T^0. The points are slightly displaced horizontally with respect to each other for clarity.

Fig. 7 : Ratio of all events to events with a forward requirement as a function of E_T^0. The points are slightly displaced horizontally with respect to each other for clarity.

Fig. 8 : Ratio $p\bar{p}/pp$ for the E_T^0 spectra for events with the forward requirement. The horizontal line at unity serves to guide the eye. Also presented as open triangles are the data from Ref. 1.

Fig. 9 : Mean charge ratio for leading particles as a function of E_T^0. The horizontal line at unity serves to guide the eye. The points are slightly displaced horizontally with respect to each other for clarity.

Fig. 10 : Mean charge asymmetry for leading particles as a function of their rapidity. The points are slightly displaced horizontally with respect to each other for clarity.

Fig. 11 : Invariant cross-section spectra for pp interactions, with shower counter and lead-glass values plotted separately. The points are slightly displaced horizontally with respect to each other for clarity. Also presented as triangles are the data from Ref. 8.

Fig. 12 : Ratio $\bar{p}p/pp$ for the inclusive neutral-cluster cross-sections as a function of p_T,

a) for lead-glass sextants,

b) for shower-counter sextants.

The horizontal line at unity serves to guide the eye.

Fig. 13 : Ratio $\bar{p}p/pp$ for the inclusive neutral-cluster cross-section as a function of p_T, for lead-glass and shower-counter data combined. The dots represent the predictions of the CIM model and the dashes those of the DQ model of Ref. 9 (see text).

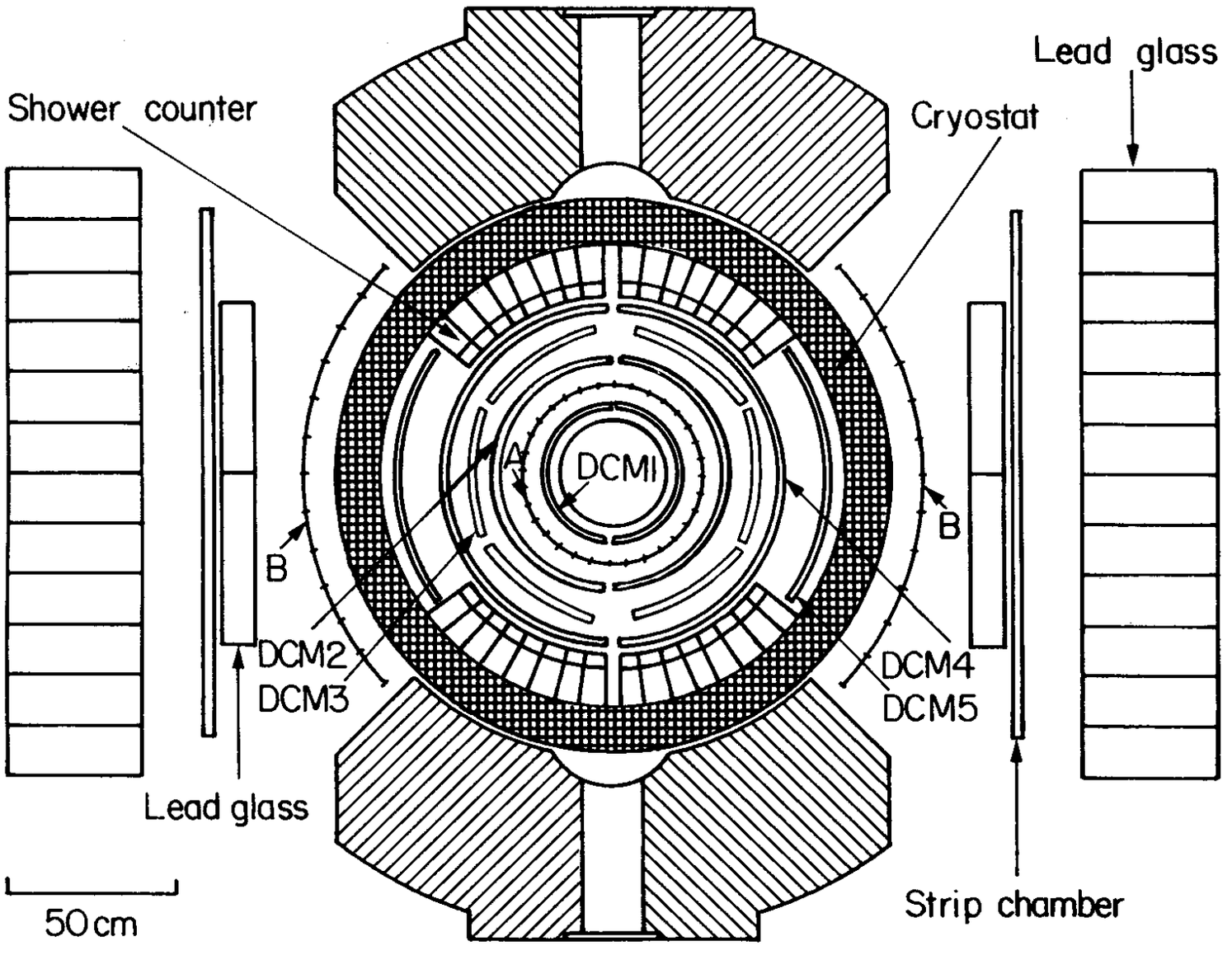
Shower counter
Lead glass
Cryostat
DCM1
A
B
B
DCM2
DCM3
DCM4
DCM5
Lead glass
Strip chamber
50 cm

Fig. 1

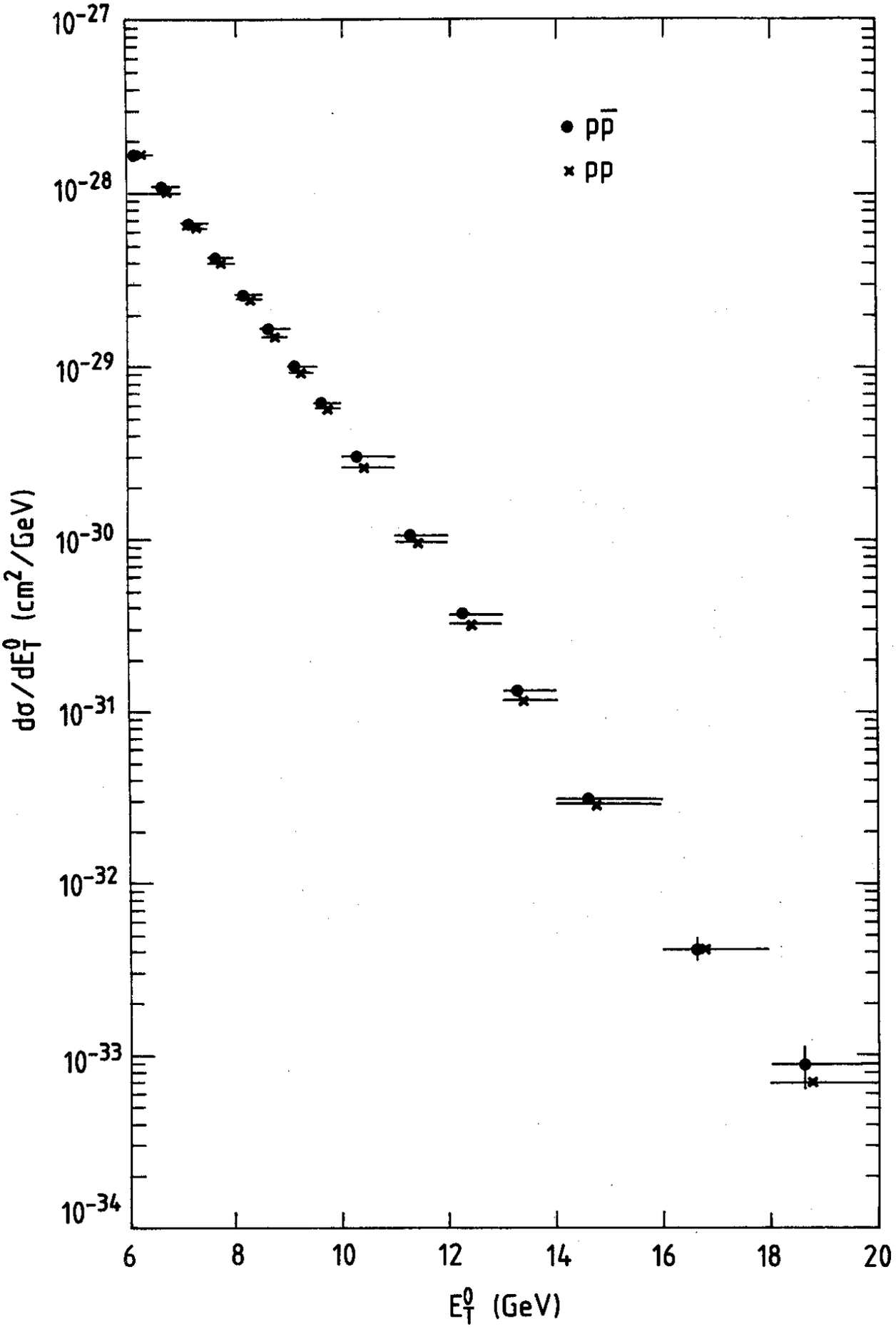
10^{-27}
10^{-28}
10^{-29}
10^{-30}
10^{-31}
10^{-32}
10^{-33}
10^{-34}
$d\sigma/dE_T^0$ (cm^2/GeV)
$p\bar{p}$
pp
6
8
10
12
14
16
18
20
E_T^0 (GeV)

Fig. 2

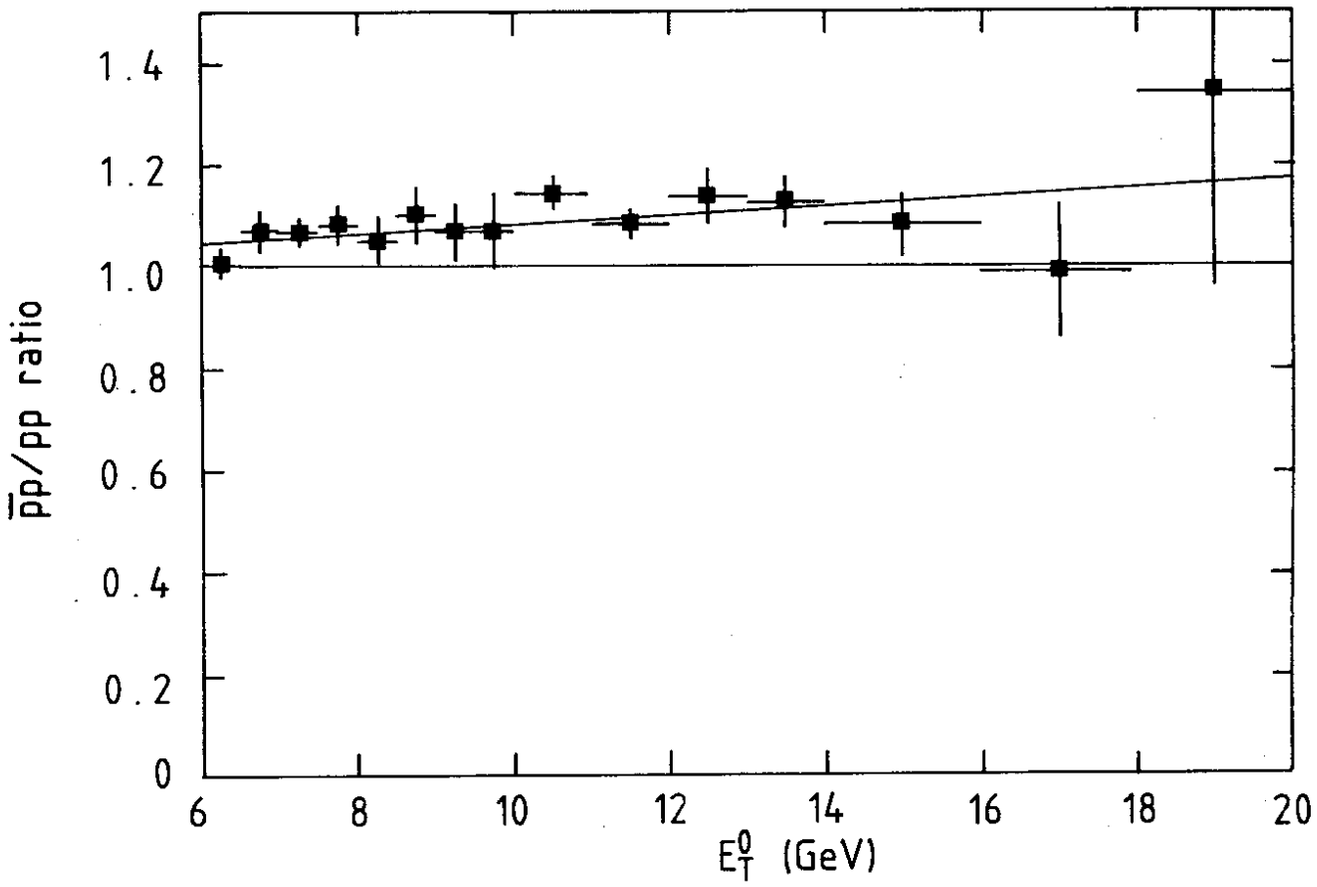
1.4
1.2
1.0
0.8
0.6
0.4
0.2
0
$\bar{p}p/pp$ ratio
6
8
10
12
14
16
18
20
E_T^0 (GeV)

Fig. 3

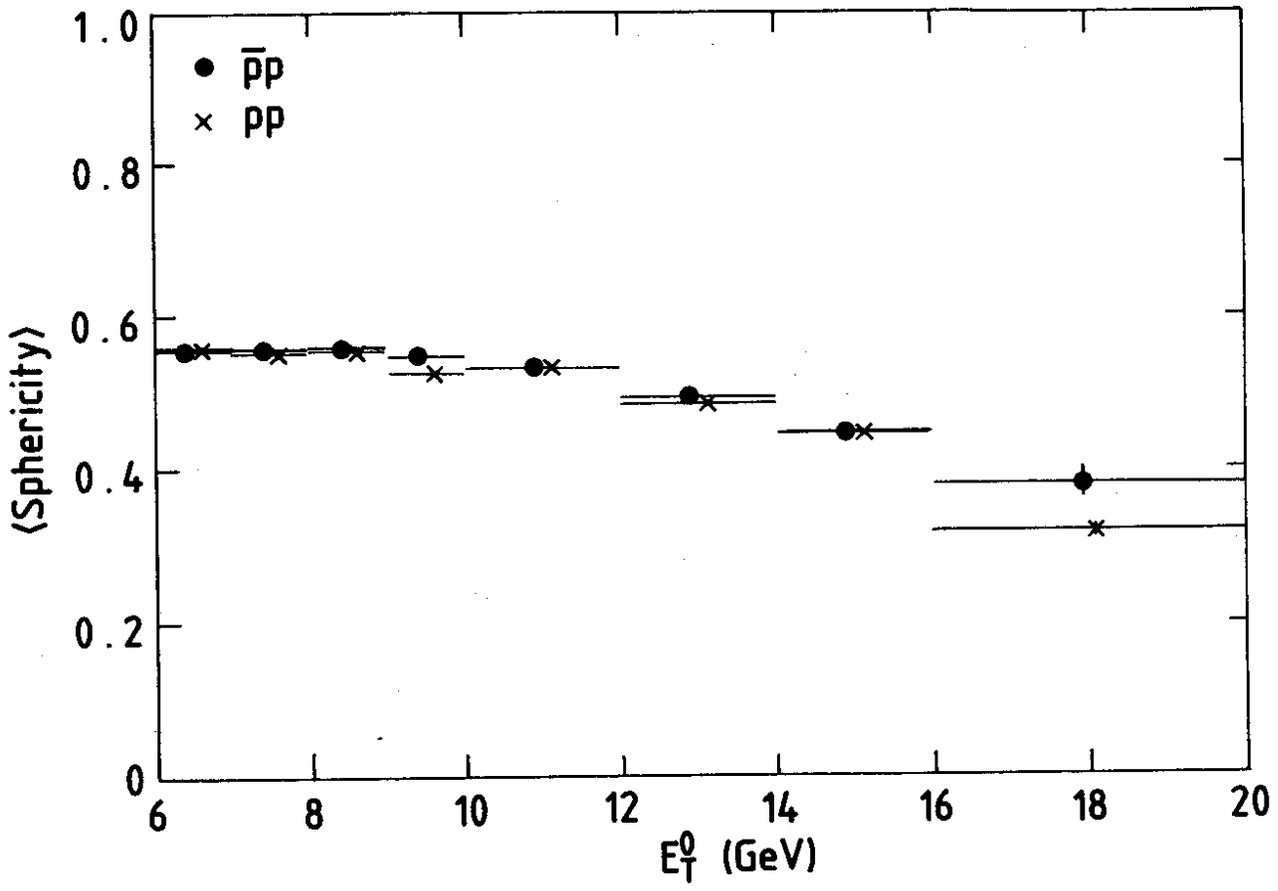
1.0
0.8
0.6
0.4
0.2
0
$\bar{p}p$
pp
⟨Sphericity⟩
6
8
10
12
14
16
18
20
E_T^0 (GeV)

Fig. 4

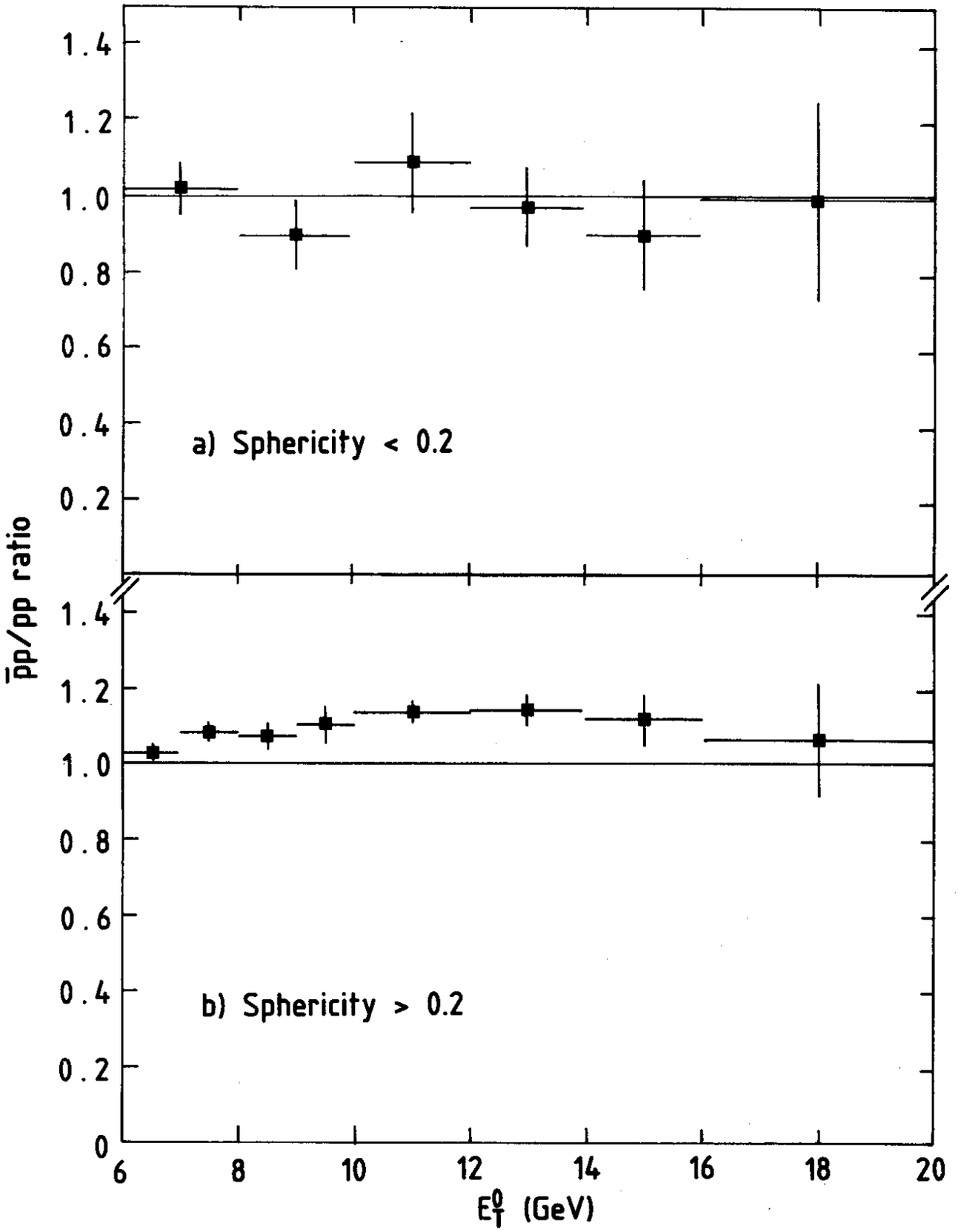
1.4
1.2
1.0
0.8
0.6
0.4
0.2
a) Sphericity < 0.2
$\bar{p}p/pp$ ratio
1.4
1.2
1.0
0.8
0.6
0.4
0.2
0
b) Sphericity > 0.2
6
8
10
12
14
16
18
20
E_T^0 (GeV)

Fig. 5

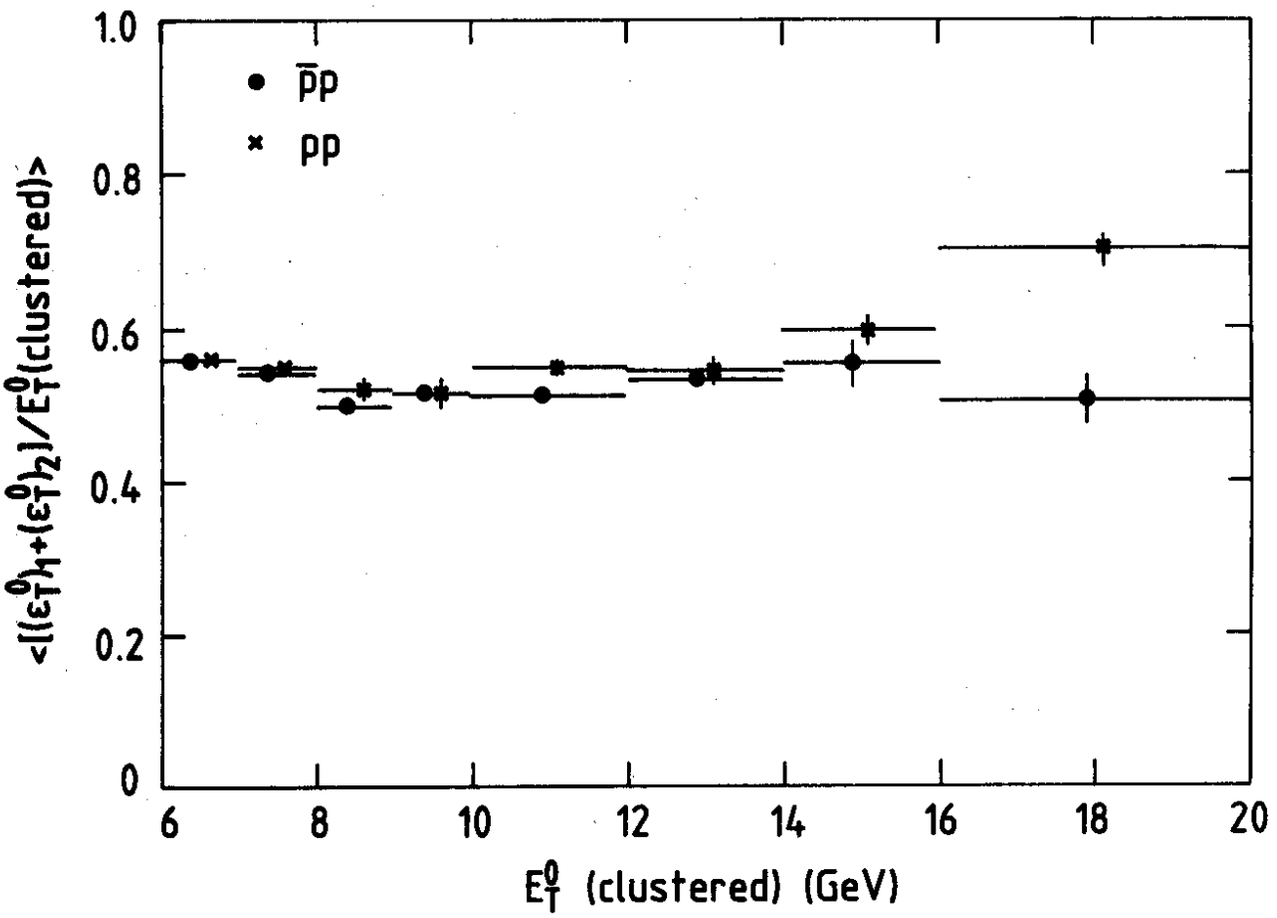
1.0
0.8
0.6
0.4
0.2
0
$\bar{p}p$
pp
$<|(\epsilon_T^0)_1+(\epsilon_T^0)_2|/E_T^0(\text{clustered})>$
6
8
10
12
14
16
18
20
E_T^0 (clustered) (GeV)

Fig. 6

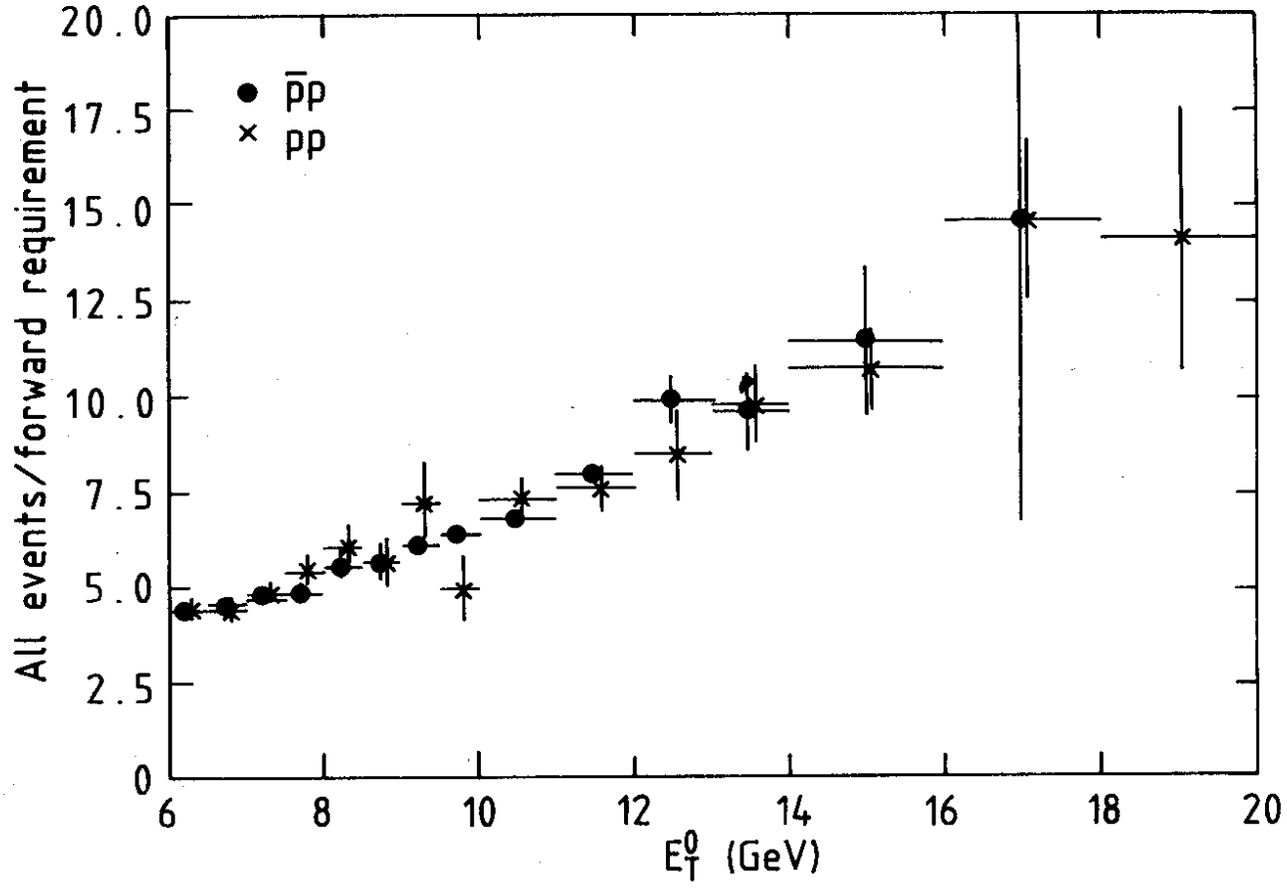
20.0
17.5
15.0
12.5
10.0
7.5
5.0
2.5
0
$\bar{p}p$
pp
All events/forward requirement
6
8
10
12
14
16
18
20
E_T^0 (GeV)

Fig. 7

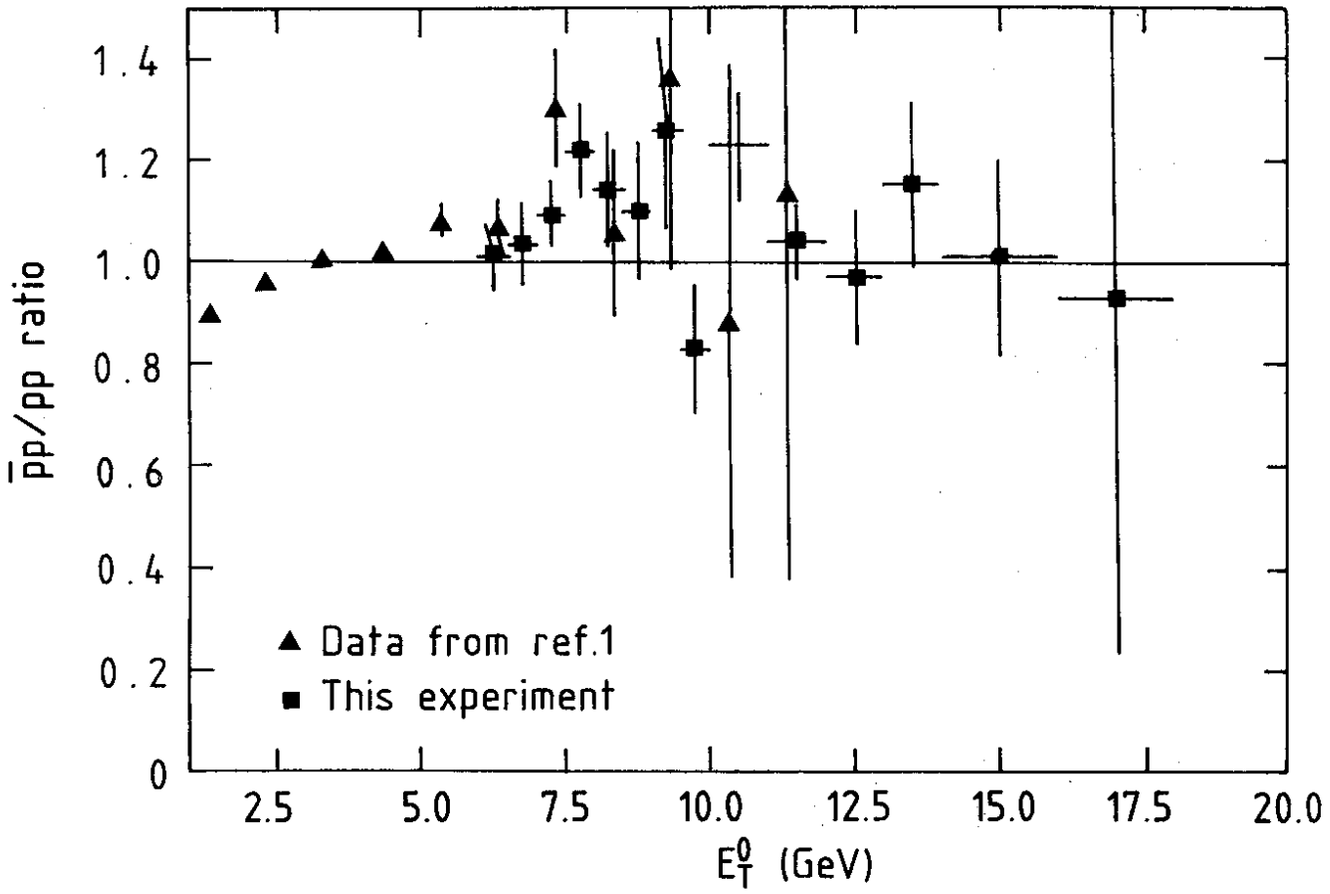
1.4
1.2
1.0
0.8
0.6
0.4
0.2
0
$\bar{p}p/pp$ ratio
▲ Data from ref.1
■ This experiment
2.5
5.0
7.5
10.0
12.5
15.0
17.5
20.0
E_T^0 (GeV)

Fig. 8

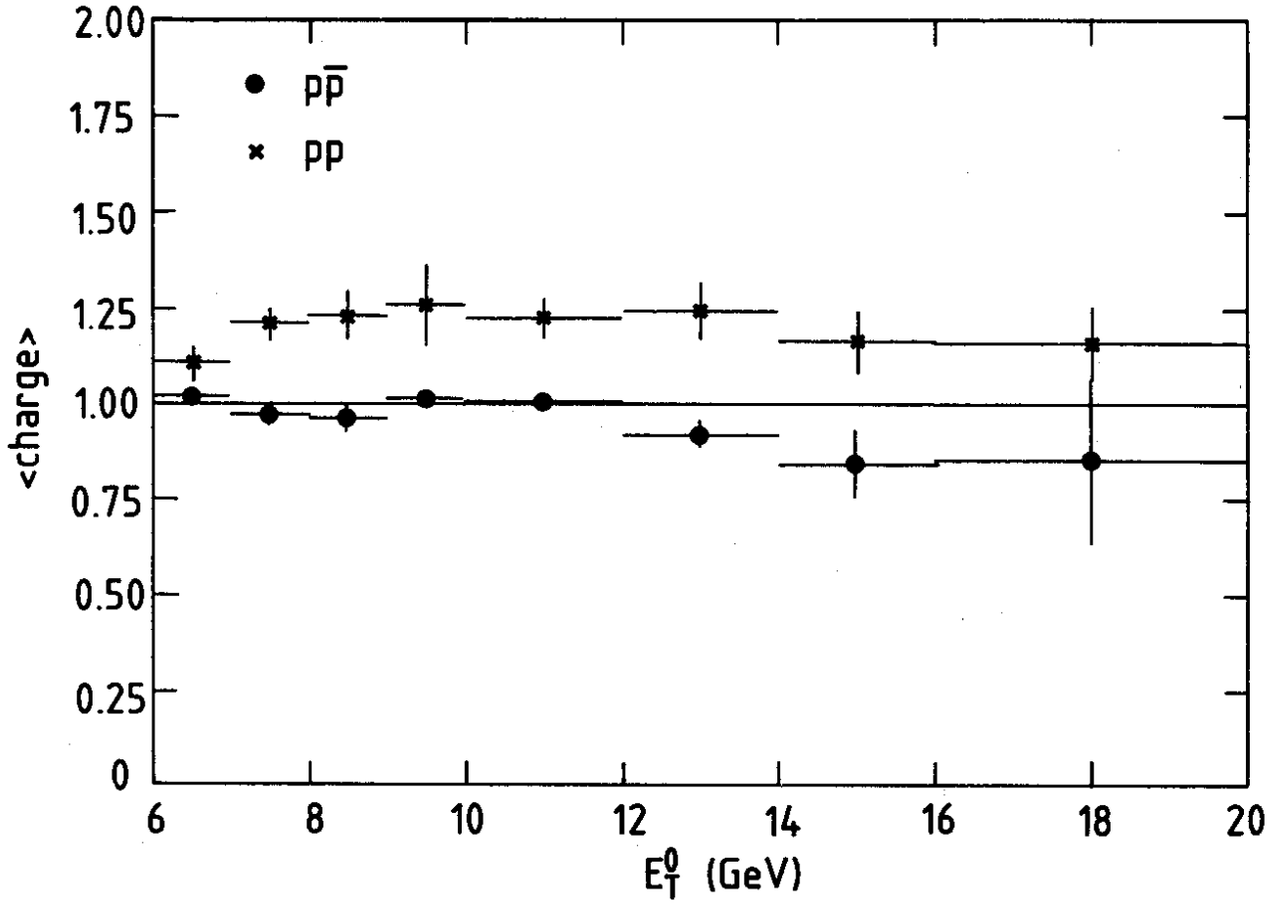
2.00
1.75
1.50
1.25
1.00
0.75
0.50
0.25
0
<charge>
● $p\bar{p}$
× pp
6
8
10
12
14
16
18
20
E_T^0 (GeV)

Fig. 9

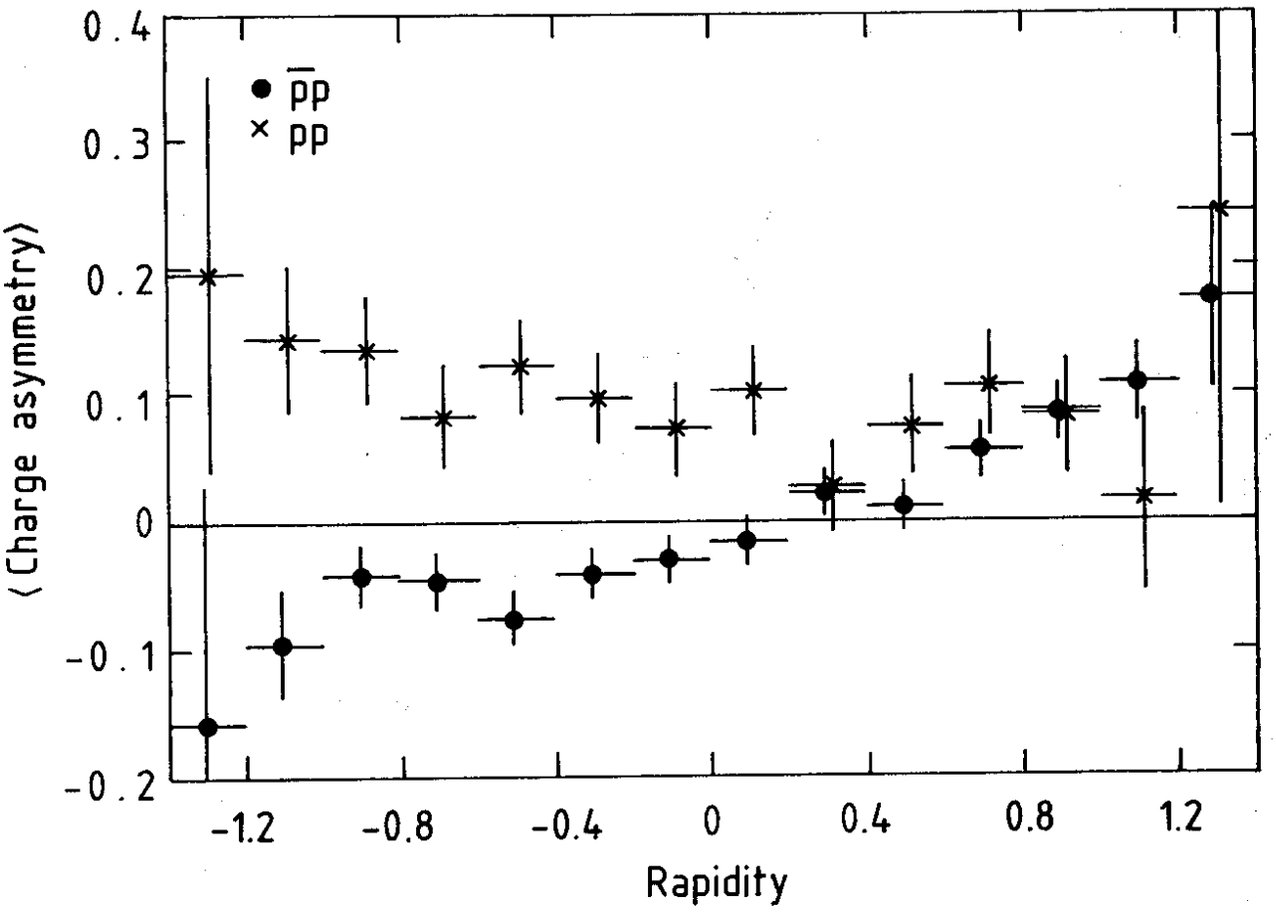
0.4
0.3
0.2
0.1
0
-0.1
-0.2
● $\bar{p}p$
× pp
⟨Charge asymmetry⟩
-1.2
-0.8
-0.4
0
0.4
0.8
1.2
Rapidity

Fig. 10

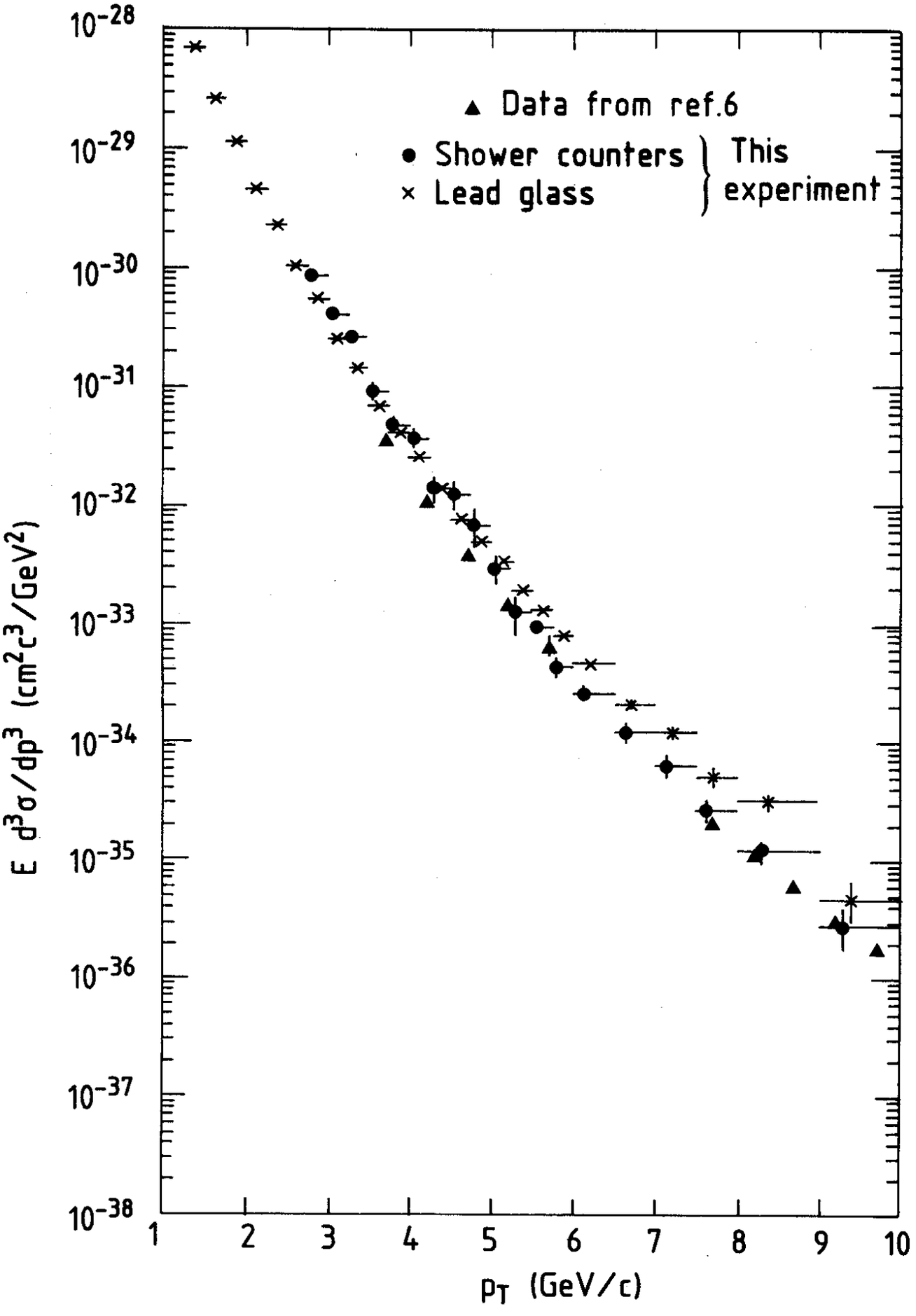
▲ Data from ref.6
● Shower counters
× Lead glass
This experiment
E d³σ/dp³ (cm²c³/GeV²)
p_T (GeV/c)
10⁻²⁸
10⁻²⁹
10⁻³⁰
10⁻³¹
10⁻³²
10⁻³³
10⁻³⁴
10⁻³⁵
10⁻³⁶
10⁻³⁷
10⁻³⁸
1
2
3
4
5
6
7
8
9
10

Fig. 11

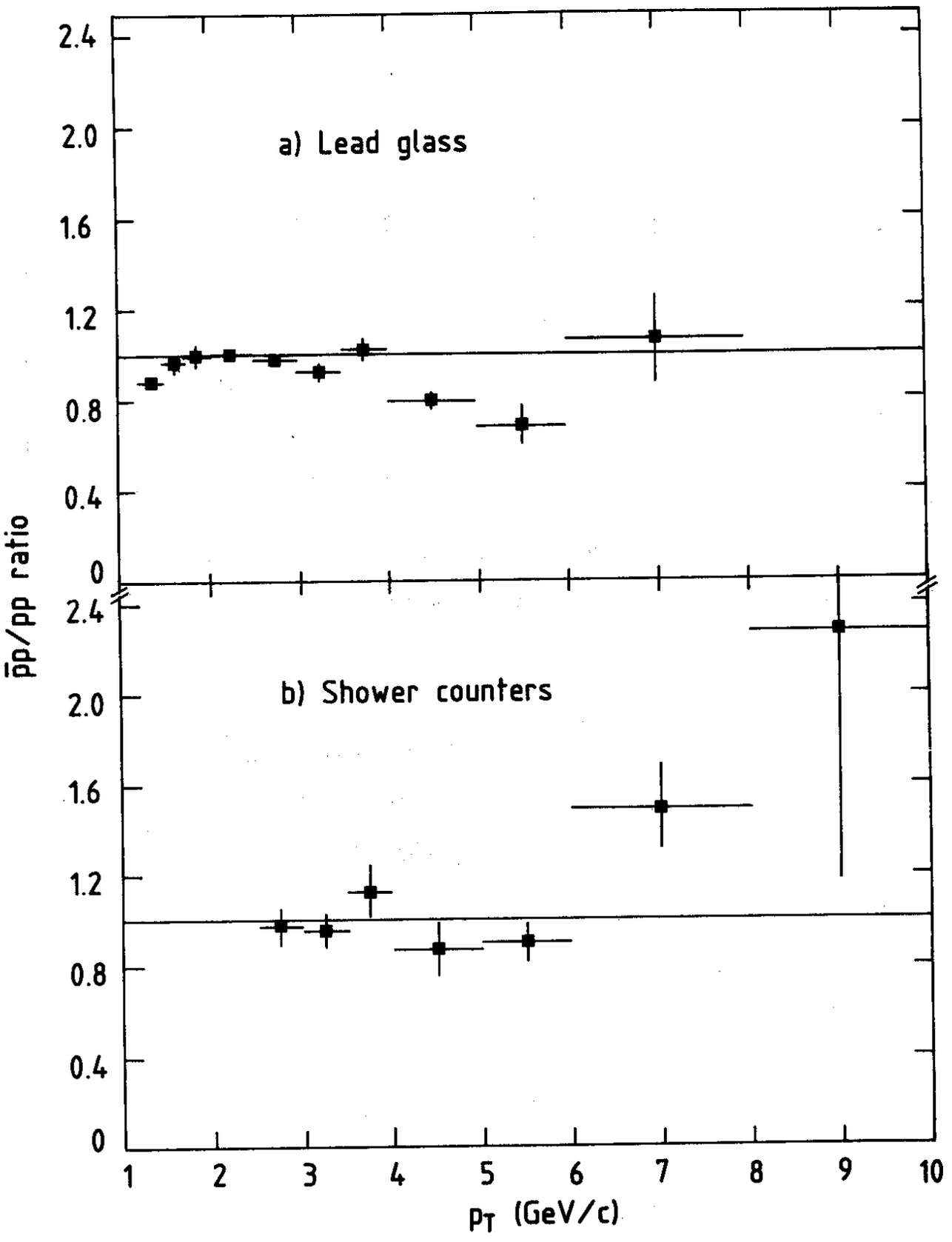
a) Lead glass
b) Shower counters
$\bar{p}p/pp$ ratio
p_T (GeV/c)
2.4
2.0
1.6
1.2
0.8
0.4
0
1
2
3
4
5
6
7
8
9
10

Fig. 12

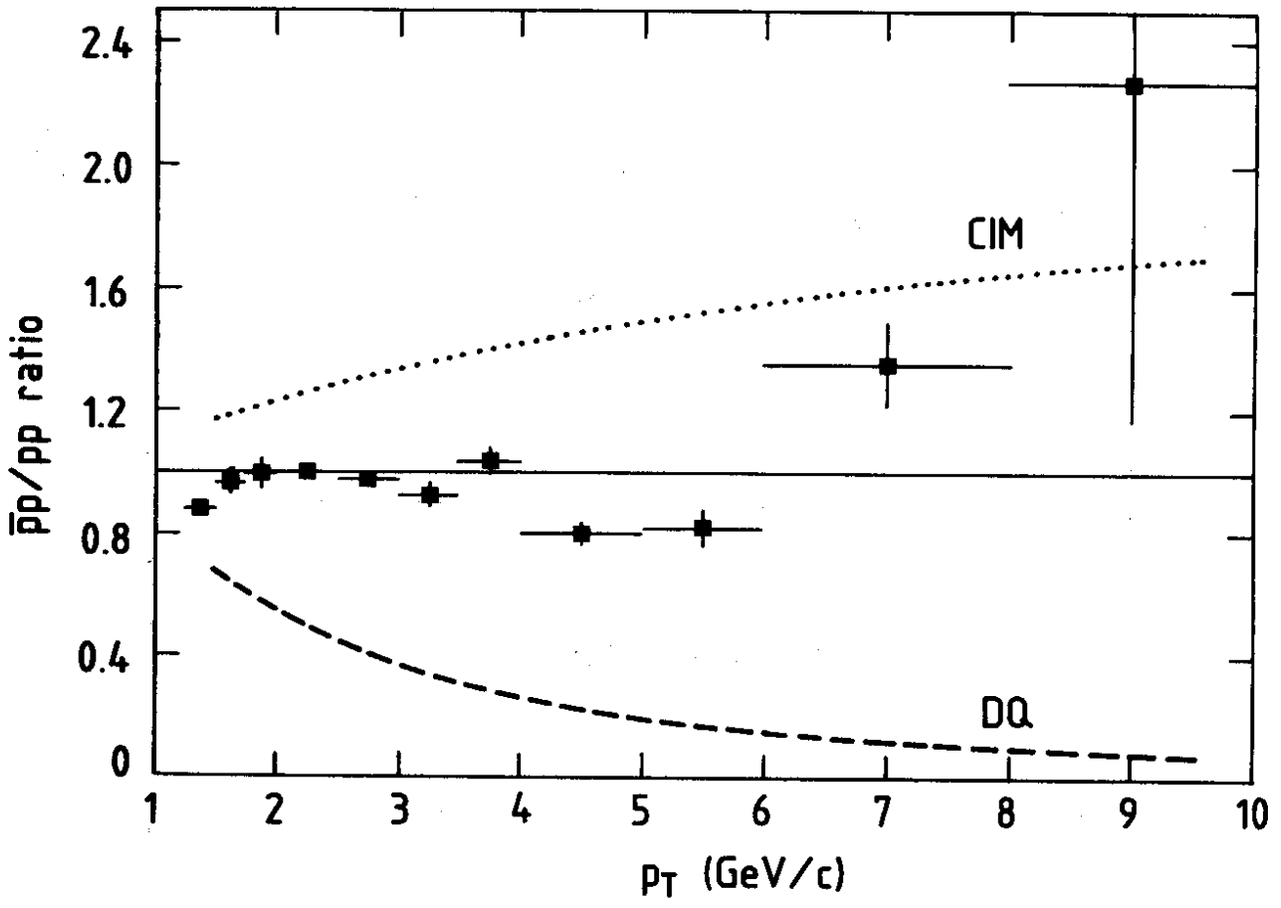

Fig. 13